Small-angle neutron scattering of percolative perfluoropolyether water-in-oil microemulsions

Small-Angle Neutron Scattering of Percolative Perfluoropolyether Water in Oil Microemulsions

M. Laurati,[†,‡] C.M.C. Gambi,[*,§,¶] R. Giordano,[⊥] P. Baglioni,[#] and J. Teixeira[||]

Laboratoire Polymères et Matériaux Avancés, CNRS/Rhodia Recherche et Technologie, 85 rue des Frères Perret, 69192 Saint-Fons Cedex, France, Polymers and Soft Matter Group, Centro de Fisica de Materiales, Universidad del Paìs Vasco, Paseo Manuel Lardizabal 4, 20018 Donostia/San Sebastiàn, Spain, Department of Physics and CNISM Via G. Sansone 1, University of Florence, 50019 Sesto Fiorentino, Florence, Italy, Deptartment of Physics, University of Messina and CNISM, Salita Sperone 31, 98010 S. Agata, Messina, Italy, Deptartment of Chemistry, University of Florence and C.S.G.I., V. G.Capponi 9, 50121 Firenze, Italy, Laboratoire Lèon Brillouin (CEA-CNRS), CEA Saclay, Gif-sur-Yvette Cedex, France, and CRS-Soft Matter (CNR-INFM), University of Rome, "La Sapienza" P.le A. Moro 2, 00185 Rome, Italy

Received: November 27, 2009; Revised Manuscript Received: February 12, 2010

A water in oil microemulsion system composed of water, surfactant, and oil, the latter two components of perfluoropolyether (PFPE) type, has been studied by small-angle neutron scattering (SANS) with the aim of knowing the microstructure of the system and to have an insight on the connection between microstructure characterization and percolation behavior. In fact, along the dilution line W/S = 11 of the phase diagram, dielectric spectroscopy and conductivity studies revealed a dynamic percolation process taking place approaching and above the dynamic percolation threshold, leading to a system composed of droplet clusters with percolation thresholds varying with temperature from a 0.501 volume fraction of the dispersed phase at 9.3 °C to 0.205 at 32.5 °C. The SANS experimental spectra of this work have been studied by modeling the microemulsion droplets as adhesive hard spheres. For all of the samples, the surfactant area per polar head has been also measured in the Porod region of the SANS spectra. Geometric and potential parameters as well as the osmotic pressure, the second virial coefficient, and the distance between droplets have been extracted from data as a function of droplets concentration. At low concentration, that is, below percolation thresholds, the droplets behave as hard spheres, whereas at threshold and above, adhesion changes significantly the samples. In fact, for each temperature, the measured size increases versus concentration from 30 to 50 Å, and the area per polar head decreases correspondingly, suggesting that a process of dynamic fusion of droplets occurs in the system above threshold, that is, couples of droplets stick and unstick continuously with interdigitation of the surfactant tails.

1. Introduction

Microemulsion systems composed of water, oil, and ionic or nonionic surfactants have been thorougly studied during the last two decades as a prototype of more complex five-component microemulsions, where the additional presence of cosurfactant and electrolyte is needed to thermodynamically stabilize the system. Such ternary microemulsions present a rich phase diagram as a function of surfactant concentration and temperature. A key parameter determining the phase behavior of such systems is the balance between the hydrophilicity and the liophilicity of the surfactant molecule. Around the hydrophile–lipophile balance temperature (HLB), ternary microemulsions typically show a so-called 2−3−1 phase evolution as a function of increasing surfactant concentration.[1] On the other hand, far from the HLB, the surfactant film acquires a curvature toward the water or the oil and two-phase coexistence of a water in oil (W/O) droplet phase and a water-rich phase, or an oil in water droplet phase and an oil-rich phase is observed. Not all ternary microemulsions follow such a phase progression though. For example, one of the most studied systems, mixtures of AOT surfactant, water, and oil, shows a large one-phase region (L2 phase) that has been identified as a water in oil droplet phase.[2,3] This droplet structure remains stable over a broad range of droplet volume fractions, extending up to the percolation threshold, and temperatures, even higher than the critical solution temperature corresponding to the cloud-point curve.[2,3] Droplet–droplet interactions have been successfully modeled by means of the square well attractive/sticky spheres potential and used to describe static, dynamic,[3] and electrical as well as mechanical transport properties.[3,4] In particular, an interesting connection between droplet cluster formation, percolation, and transport properties has been established. Approaching percolation, clusters of droplets are formed which grow in size until they span the sample volume. When this happens, a sudden increase in the conductivity and viscosity of the system is observed,[3] corresponding to formation of conducting channels of droplets and load-bearing transient networks. One question that remains open, despite the substantial amount of knowledge already accumulated on this system, is how the structure evolves beyond percolation and how this affects the transport properties of the system.

* To whom correspondence should be addressed.
† CNRS/Rhodia Recherche et Technologie.
‡ Universidad del Paìs Vasco.
§ University of Florence.
⊥ University of Messina and CNISM.
University of Florence and C.S.G.I.
|| CEA Saclay.
¶ University of Rome.

10.1021/jp911278j
Published on Web 03/03/2010

A ternary microemulsion system showing many analogies with the one formed by AOT surfactants is a mixture of ammonium salts of perfluoropolyether (PFPE) carboxylates, water, and PFPE oil. Ammonium salts of perfluoropolyether (PFPE) carboxylates are very effective surfactants for the preparation of monophasic, transparent, isotropic microemulsions. Oil-soluble long-chain PFPE surfactants form water in oil (W/O) ternary microemulsions, without cosurfactant, as reported in ref 5. The microemulsions system composed of water, PFPE surfactant of molecular weight 710, and PFPE oil of molecular weight 900 has been intensively investigated using several techniques.[5−18] No O/W microemulsion region was found in the phase diagram.[5] On the contrary, the W/O monophasic microemulsion region was quite large. It extended from a very low water to surfactant ratio (W/S) up to W/S = 22 (molar ratio) and from very dilute samples up to dense samples with maximum ϕ (volume fraction of the dispersed phase) values, 60% at W/S = 2.3, 75.7% in the W/S range from 5.6 to 11, and 50% at W/S = 20.[5] The volume fraction ϕ is defined as the ratio of water plus surfactant volume over the total volume (water, surfactant, and oil), assuming that the dispersed phase is composed of water droplets coated by surfactant molecules.

Previous structural investigations by static and dynamic light scattering (SLS and DLS) and small-angle neutron scattering (SANS)[6,7,14,15] gave insight into the system's microstructure for dilute microemulsions. In particular, DLS measurements showed that the hydrodynamic radius of the droplets increased from 27 to 57 Å while increasing the W/S ratio from 6.5 to 22. Also, the radius remained constant up to increasingly higher volume fractions when increasing the W/S ratio (up to 5% at W/S = 6.5; up to 40% at W/S = 22). Here, the hydrodynamic radius represents the whole aggregate, that is, the inner water core and the interfacial layer composed of surfactant and some oil molecules trapped between surfactant tails. By DLS, droplets with hydrodynamic radii of 27, 31, 44, 57 Å at W/S = 6.5, 11, 16, and 22, in a ϕ range lower than 5, 10, 20, and 40%, respectively, were found.[7] In addition, it was also found[7] that droplets interact via steric repulsion combined with an attractive interaction that becomes more important for lower W/S ratios. The second virial coefficient of the attractive component was −20 (very adhesive droplets) at W/S = 6.5, and it decreased to −8 at W/S = 11, −2 at W/S = 16, and 0 at W/S = 22.[7]

SANS measurements in the dilute regime were used to estimate the radius of the droplet's aqueous core. From a Guinier analysis, it was found that the radius increases from 23 to 36 Å with increasing W/S from 11 to 20.[14,15] Furthermore, it was found that the area per polar head decreases while increasing ϕ at a constant W/S (=11) ratio. This means that the packing of the surfactant in the droplet increases with increasing ϕ. The latter trend was confirmed at two different temperatures, 20 and 35 °C.[14] SANS analysis at W/S = 15 and 20 (20 °C) was also showing[18] that the microemulsion system is composed of polydispersed spheres with an aqueous hard core of average diameter 60−70 Å at W/S = 20 and 55−60 Å at W/S = 15, in both cases with a polydispersity of 20%. Excluding one sample (the ϕ = 0.0318 sample at W/S = 20), all other samples present attractive interactions which can be modeled by an adhesive potential of width $\Delta \approx 7$ Å and depth u_0 less than $10k_BT$ units.

Overall, trends of structural changes obtained by SANS agree quite well with DLS results when taking into account that the hydrodynamic diameter measured by DLS is larger than the average aqueous hard-sphere diameter obtained by SANS.

In the W/O microemulsions at W/S = 11 of this work, as for W/S = 15 and 20 already studied, we should expect three regions differing for the scattering length density and two contrast values because of the water core, the interfacial shell composed of carboxylate groups of PFPE surfactant molecules plus some oil molecules, and the continuous medium composed by PFPE oil. However, as the scattering length density of the surfactant heads, $CO_2^-NH_4^+$, is the same as that of the surfactant tails and both are equal to the scattering length density of the oil molecules (3.88×10^{10} cm^{-2}), it remains one contrast 18.3×10^{20} between the water core and PFPE compounds.

In this paper, we investigate in more detail microstructural changes of this microemulsion system as a function of increasing volume fraction of the dispersed phase along the dilution line W/S = 11. Compared to previous work, the present study covers a quite large domain of concentrations (from 0.0205 to 0.757), extending in particular our investigation to the region of high concentrations. When approaching this region of large volume fractions of dispersed phase, the system viscosity increases strongly,[5] leading to a state of partial gelification which can be associated with a percolation phenomenon driven by aggregation.

Previous studies used Ohmic conductivity and dielectric spectroscopy to investigate the percolation phenomenon at several W/S ratios (including W/S = 11) and over a broad range of temperatures. From these measurements, the scaling exponents below and above the percolation threshold were calculated.[11−13,17]

By the concentration dependence of the static dielectric constant and Ohmic conductivity, by the frequency dependence of the complex dielectric constant real part and of the loss angle tangent, as well as by the temperature dependence of the static dielectric constant and Ohmic conductivity, it was found that percolation is dynamic below and above the respective percolation thresholds. Concentration, thermal, and frequency ranges explored were ϕ = 0.205−0.501, T = −10−+45 °C, and f = 100 kHz−13 MHz. In the dilute region, the conduction mechanism of noninteracting droplets was interpreted in terms of droplet charge fluctuations.[19,20] Approaching the percolation threshold, the formation of transient clusters was found to occur because of attractive interactions between droplets. The exchanges of ionic species between droplets were favored by the ability of the interfacial layers to interpenetrate significantly; thus surfactant ions and counterions migrated from droplets to droplets within a cluster.

From the latter investigation, it was hypothesized that clusters of droplets change in number density and size as a function of both the total number density of droplets and temperature, without an important internal modification of the cluster's structure, which seems to be composed of strongly interacting droplets.

The main goal of this study is therefore to confront this picture with a systematic analysis of the structure on the droplet size scale as a function of increasing volume fraction. This is obtained by performing SANS experiments on samples preceding, approaching, and beyond the percolation boundary. To describe our data, we use a microemulsion model of polydispersed spherical droplets interacting via a steric plus sticky hard-sphere potential. This potential, or Baxter's potential, has found applications in characterizing the structure and thermodynamic properties of sterically stabilized silica colloidal droplets,[21,22] microemulsion systems,[3,23−25] and nonionic micellar solutions.[26] All of these systems consist of droplets interacting via very short-range attractive potentials superimposed to the hard-sphere repulsion potential. In order to investigate surfactant packing

effects, the area per polar head was also measured for all of the samples in the Porod region of the spectra. Dilute samples at W/S = 11 were accurately described by the Baxter potential, whereas close to the percolation threshold, the Baxter model is not enough accurate to fit the experimental spectra. For dense samples, the Baxter model of the Microemulsion Model section is approximate in the sense that it gives the main information such as the droplet diameter, the distance between neighbors, and approximate values of the potential parameters. The qualitative description of the system is justified by the fact that at such high concentrations, percolation plays an important role that cannot be taken into account by the Baxter potential. Above the percolation threshold, the changes in the microemulsion system are important. The landscape of the system changes from adhesive droplets below percolation threshold to formation of dynamic clusters of droplets above. However, the Baxter potential seems appropriate for particles in contact.

2. Microemulsion Model

In modeling the microemulsion, we assumed that the system is composed of droplets with an aqueous spherical hard core of diameter σ and an attractive shell of thickness Δ outside of the core. The attraction between droplets is generally found in water in oil microemulsions and has its origin in the adhesion forces that arise between the tails of the surfactants when they overlap.[27,28] The interactions between droplets in solution were described by means of the Baxter potential.[29,30] The Baxter potential is a pair square well potential of the form

$$\gamma u(r) = \begin{cases} +\infty & r < \sigma \\ -u_0 = -\ln\left[\dfrac{a}{12\tau(a-\sigma)}\right] & \sigma < r < a \\ 0 & r > a \end{cases} \quad (1)$$

where $\gamma = 1/k_BT$ (k_B is the Boltzman's constant, and T the absolute temperature), σ is the diameter of the aqueous spherical hard core, Δ is the potential well width (of depth $-u_0$), $a = \sigma + \Delta$ is the overall range of the potential,[3,30,31] and $1/\tau$ is the so-called stickiness parameter, defined as[3,30]

$$\frac{1}{\tau} = \frac{12\Delta}{a}\exp(\gamma u_0) \quad (2)$$

According to eq 2, the droplet stickiness increases as Δ/a or γu_0 increase. In the limit of an infinitely thin ($\sigma \to a$) or infinitely deep ($u_0 \to \infty$) well, τ tends to infinity and the hard-sphere potential is recovered. For AOT (sodium bis(2-ethylexyl)sulphosuccinate) water in decane microemulsions, the authors of ref 30 declare that the Δ parameter should correspond to the length of the hydrocarbon tail, and the tail could take an increasing stretched conformation as the temperature increases.

The structure factor $S(Q)$ for droplets interacting through the Baxter potential can be calculated in the analytical form in the limit $\sigma \to a$, according to the original work of Baxter.[29,30] More recently, following a perturbative approach, Menon has shown[31] that an analytical expression for $S(Q)$ can be obtained for small but finite values of Δ/a, relaxing the Baxter assumption $\Delta \to 0$ and $u_0 \to \infty$. In this approach, the structure factor has the following expression

$$S(k)^{-1} = A^2(k) + B^2(k) \quad (3)$$

where $k = Qa$ and

$$A(k) = 1 + 12\eta\left[\alpha\left[\frac{\sin(k) - k\cos(k)}{k^3}\right] + \beta\left[\frac{1-\cos(k)}{k^2}\right] - \frac{\lambda}{12}\cdot\frac{\sin(k)}{k}\right]$$

$$B(k) = 12\eta\left[\alpha\left[\frac{1}{2k} - \frac{\sin(k)}{k^2} + \frac{1-\cos(k)}{k^3}\right] + \beta\left[\frac{1}{k} - \frac{\sin(k)}{k^2}\right] - \frac{\lambda}{12}\left[\frac{1-\cos(k)}{k}\right]\right]$$

with

$$\alpha = \frac{1+2\eta-\mu}{(1-\eta)^2} \qquad \beta = \frac{-3\eta+\mu}{2(1-\eta)^2} \qquad \mu = \lambda\eta(1-\eta)$$

The parameter η is given by $\eta = \pi\rho a^3/6$, where ρ is the number density of droplets. η represents the volume fraction of the phase contained in the $\sigma + \Delta$ spherical droplets region of the microemulsion system, that is, the hard-sphere region plus the adhesive region. The η parameter corresponds to the volume fraction of sticky spheres. Such a quantity will therefore be always smaller than the total volume fraction of water + surfactant since a sticky sphere is mainly formed by the water core plus an additional shell of relatively small volume (short-range attraction). The additional shell will contain only a fraction of the volume occupied by the surfactant. λ is an undetermined parameter that satisfies the quadratic equation

$$\lambda\tau = \frac{\eta\lambda^2}{12} - \frac{\eta\lambda}{1-\eta} + \frac{\frac{1+\eta}{2}}{(1-\eta)^2} \quad (4)$$

The droplets were considered to be polydispersed in size, and their size distribution was modeled by means of the Schultz distribution function.[32,33]

The SANS intensity (coherent scattering cross section of neutrons per unit volume of the sample) for a system of polydispersed spherical water droplets, having a Schultz distribution in size, can be expressed as in ref 3

$$I(Q) = \Delta\rho^2 \cdot V_{HS} \cdot \phi_w \frac{(Z+6)(Z+5)(Z+4)}{(Z+1)^3} P(Q) \cdot S'(Q) \quad (5)$$

where $\Delta\rho^2$ (contrast factor) is the square of the difference between the scattering length densities of water and fluorinated compounds, $V_{HS} = \pi\sigma^3/6$ is the aqueous spherical hard-core region of the droplet, and ϕ_w is the water volume fraction of the sample, which is known from the sample composition. Z is the width parameter of the Schultz distribution[32,33] that leads to estimate the size polydispersity, poly $= 1/(Z+1)^{1/2}$. $P(Q)$ is the normalized, spherical size-averaged droplet form factor, defined as

$$P(Q) = \frac{1}{\langle R^6\rangle}\left\langle R^6\left(\frac{3j_1(QR)}{QR}\right)^2\right\rangle \quad (6)$$

where $R = \sigma/2$ is the hard-sphere radius, $j_1(X)$ is the first-order spherical Bessel function, and the brackets indicate the average over the size distribution. $S'(Q) = 1 + \beta(Q)[S(Q) - 1]$ is the apparent interdroplet structure factor, following the approach of Kotlarchyk and Chen.[32] $S(Q)$ is the average one-component structure factor, which in our case is calculated according to eq 3. The factor $\beta(Q)$, whose value varies between 0 and 1, is responsible for suppressing the true structure factor oscillations in a system of polydisperse droplets.[32]

In this model, $I(Q)$ depends on four independent parameters, σ, Δ, u_0, and Z. In the fitting procedure, the contrast was fixed to the value calculated in the Introdction section on the basis of the chemical composition of the components. Furthermore, each droplet contributes to the volume fraction through the aqueous hard-sphere core plus a shell with the surfactant tails covering the droplet. The stickiness between droplets we expect to be due to adhesion between the surfactant tails of neighboring droplets or portions of the surfactant tails.

Under this hypothesis, $\eta = ((\sigma + \Delta)^3/\sigma^3)\phi_w = (\pi/6)\rho a^3$ depends on two fitting parameters σ and Δ and the known composition parameter ϕ_w. Of note, $\eta > \phi_w$ for adhesive microemulsions. In fact, only when $\Delta = 0$, it is $\eta = \phi_w$.

Finally, in order to correct for data smearing due to resolution effects, in the fitting procedure, we convoluted the theoretical model with a resolution function, calculated according to the work of Pedersen et al.[34]

3. Experimental Section

The ternary water in oil microemulsion is composed of an ammonium carboxylate PFPE surfactant of molecular weight 710 and a PFPE oil of molecular weight 900. The density and viscosity of the PFPE oil are 1.8 $g \cdot cm^{-3}$ and 6.2 cP,[11] respectively. The sample preparation was described in ref 5. The fluorinated compounds were provided by Ausimont SpA (now Solvay Solexis), Milan, Italy. The water was taken from a Millipore Milli-Q system.

The surfactant tail and the oil molecule have a similar composition $R_e-[O-CF_2-C(CF_3)F]_n-OCF_2-R_h$ as detailed in refs 11−15. The R_e terminator is a mixture of CF_3, CF_3CF_2, and $(CF_3)CF$ groups. In the oil molecule, R_h is equal to R_e, and in the surfactant molecule, R_h represents the ammonium carboxylate group $CO_2^-NH_4^+$.

The SANS measurements have been performed on the PAXE spectrometer of the Laboratoire Léon Brillouin at Saclay (France) using a wavelength of 5 Å with a wavelength spread of 10%. The Q range investigated, for all of the samples, was from 0.02 to 0.28 $Å^{-1}$ (sample to detector distance fixed at 2.515 m). Collimation was realized by two circular slits, one of 7 mm diameter in front of the sample, defining the area and the scattering volume of the sample, plus a second one of 14 mm diameter placed 2.5 m far from the first slit, in the direction of the incoming neutron flux.

Samples of thickness 1 mm were contained in flat quartz cells, temperature-controlled within ±0.1 °C. The temperature of the measurements was 20 °C. Standard procedures have been used to reduce the data to absolute units.[35] The intensity was corrected for the empty cell contribution and normalized to the absolute scale by means of a direct measurement of the intensity of the incoming beam.[35] The contribution of the PFPE oil was subtracted.

In the data analysis performed by the computer, a nonlinear fitting procedure by means of the Minuit program of the CERN library was performed on the experimental spectra and the $I(Q)$ in the form of a Fortran function written by us.

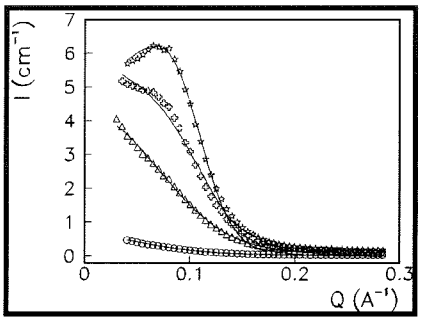

Figure 1. Experimental spectra of the samples at W/S = 11 and 20 °C for $\phi = 0.0205$ (circles), 0.205 (triangles), 0.327 (crosses), and 0.408 (stars). Fitted curves by the AHS model. The error bars (standard deviations) are reported on all of the figures of this paper, except when they are smaller than the symbols used.

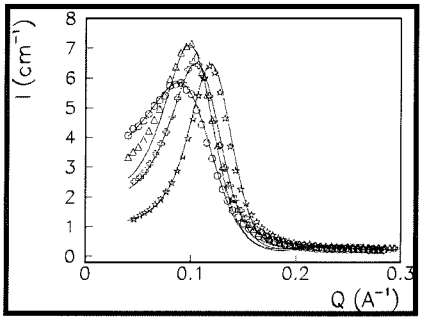

Figure 2. Experimental spectra of the samples at W/S = 11 and 20 °C for $\phi = 0.501$ (circles), 0.600 (triangles), 0.644 (crosses), and 0.757 (stars). Fitted curves by the AHS model. The error bars (standard deviations) are reported on all of the figures of this paper, except when they are smaller than the symbols used.

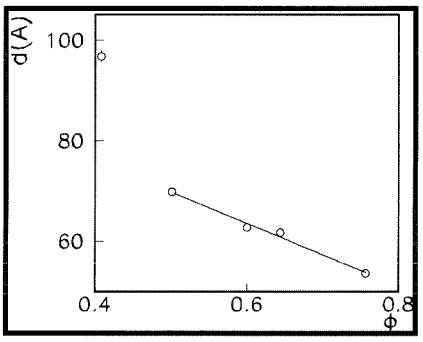

Figure 3. Distance between neighboring droplets versus ϕ for dense samples.

4. Results

Figures 1 and 2 show the 20 °C experimental spectra of samples at W/S = 11 with ϕ in the range of 0.0205−0.757. The samples span from the very dilute region, a few percent of the dispersed phase, to the most dense monophasic sample, 75.7% of dispersed phase.

In the denser samples, we calculated the distance between neighboring droplets from the position of the scattering intensity peak, that is, as $2\pi/Q_{max}$, where Q_{max} is the Q value corresponding to the peak maximum. The distance plotted versus ϕ in Figure 3 for samples in the range of 0.408−0.757 with distances from 53.6 Å at 0.757 to 69.8 Å at 0.501 shows a linear trend. The distance at 0.408 is not compatible with the other values of the linear trend, pointing to a discontinuity due to the percolation threshold. It is worth noting that the 53.6 Å value is the maximum size of particles at W/S = 11 of the monophasic microemulsion.

As a first step in modeling the experimental spectra, we investigated the Porod region of each spectrum. In fact, at high

TABLE 1: SANS Results at W/S = 11 and T = 20 °C, Results by the AHS Model with Four Free Parameters, σ, poly (polydispersity), Δ, and u_0 and η Calculated as the Reduced χ^2 of the Fit and the Interfacial Area Per Polar Head Σ

ϕ	ϕ_w	ϕ_s	σ Å	poly	Δ Å	$u_0\ k_bT$	η	χ^2	Σ Å^2
0.0205	0.00687	0.01363	30.8 ± 0.5	0.34	0 ± 5	0 ± 3	ϕ_w	5	44 ± 2
0.205	0.0687	0.1363	32.9 ± 0.8	0.33	0 ± 0.1	0 ± 3	ϕ_w	2	45 ± 3
0.327	0.1096	0.2174	46.0 ± 0.3	0.11	1.3 ± 1.6	0 ± 7	ϕ_w	59	37 ± 3
0.408	0.1367	0.2713	50.2 ± 0.2	0.00	2.5 ± 0.4	−4 ± 2	0.1582	7.5	36 ± 1
0.501	0.1678	0.3332	49.2 ± 0.4	0.00	4.7 ± 0.5	−3.2 ± 0.5	0.2206	6.1	33 ± 0.5
0.600	0.2011	0.3989	49.8 ± 1	0.00	6.2 ± 0.9	−4.5 ± 1	0.286	30	29 ± 1
0.644	0.2158	0.4282	48 ± 1.5	0.00	6.1 ± 0.5	−6 ± 3	0.309	28	32 ± 2
0.757	0.2537	0.5033	45.4 ± 1	0.00	6.5 ± 0.7	−8 ± 2	0.379	41	31 ± 2

Q, all of the spectra follow the Porod law[36] $Q^4I(Q) = A + BQ^4$, where $A = 2\pi\Delta\rho^2 c_s\Sigma$, with c_s as number of surfactant molecules per unit volume of the sample, Σ as area per polar head group of the surfactant molecules at the droplet interface, and B as background due to the incoherent part of the signal. When this law applies, the interfacial region of the droplets is sharp. We are assuming that all of the surfactant molecules are at the surface of the droplets.

Since c_s is known from the sample composition and $\Delta\rho^2$ is fixed to the value calculated in the Introduction section, by means of the A parameter, we can calculate the area per polar head for each sample. The obtained values are reported in Table 1. In the range ϕ = 0.205−0.600, a figure of Σ versus c_s at 20 and 35 °C was already depicted in ref 14. The background calculated by the Porod law was then subtracted from each spectrum before performing any further analysis of the experimental data.

As suggested from previous studies,[11] the percolation threshold at 20 °C is $\phi_p \approx 0.4$. In order to have better insight into the structural evolution of the system close to the percolation threshold, additional SANS measurements in the thermal range of 10−35 °C were performed for samples with ϕ = 0.205, 0.327, 0.408, and 0.501. In fact, with increasing temperature, the percolation threshold ϕ_p decreases from ϕ_p = 0.501 at 9.3 °C to ϕ_p = 0.408 at ~20 °C to ϕ_p = 0.205 at 32.5 °C.[11] The spectra are reported in Figures 4−8. In the whole thermal range, the presence of large-scale aggregates is evidenced by the high level of the intensity scattered at low Q.

For the spectra at different temperatures, the Porod region was analyzed as for the samples at 20 °C, the background was subtracted before any fitting procedure to theoretical models, and the area per polar head was calculated. The obtained values are reported in Table 2.

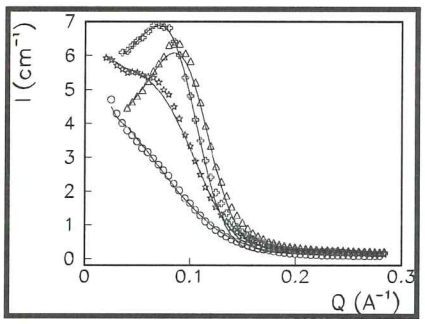

Figure 4. Experimental and fitted curves with the AHS model at T = 10 °C with ϕ = 0.205 (circles), 0.327 (triangles), 0.408 (crosses), and 0.501 (stars).

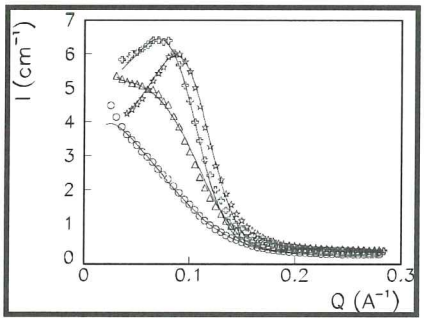

Figure 5. Experimental and fitted curves with the AHS model at T = 16. 5 °C with ϕ = 0.205 (circles), 0.327 (triangles), 0.408 (crosses), and 0.501 (stars).

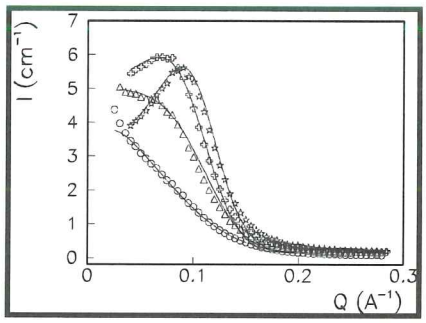

Figure 6. Experimental and fitted curves with the AHS model at T = 25 °C with ϕ = 0.205 (circles), 0.327(triangles), 0.408(crosses) and 0.501(stars).

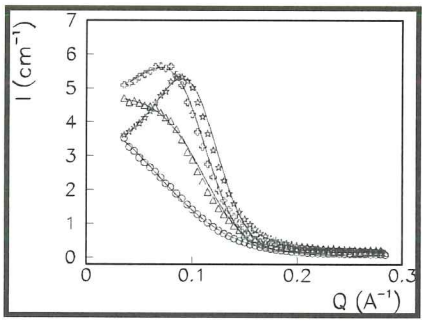

Figure 7. Experimental and fitted curves with the AHS model at T = 30 °C with ϕ = 0.205 (circles), 0.327 (triangles), 0.408 (crosses), and 0.501 (stars).

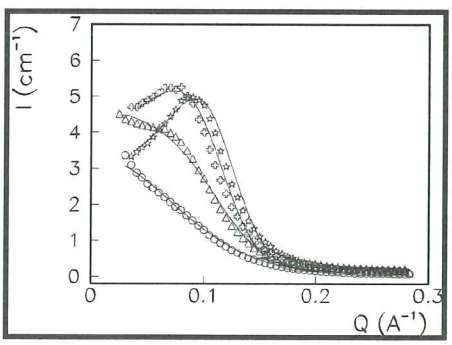

Figure 8. Experimental and fitted curves with the AHS model at T = 35 °C with ϕ = 0.205 (circles), 0.327 (triangles), 0.408 (crosses), and 0.501 (stars).

TABLE 2: SANS Results at W/S = 11 and T = 10−35 °C along with Results by the AHS Model with Four Parameters, χ^2 of the Fits, and Σ

ϕ	σ Å	poly	Δ Å	u_o k_bT	χ^2	Σ Å^2
T = 10.0 °C						
0.205	36.4 ± 0.5	0.26	0 ± 0.5	0 ± 2	44	47 ± 3
0.327	48 ± 1	0.12	2 ± 1	−4 ± 2	42	37 ± 3
0.408	54 ± 2	0.10	6 ± 2	−4 ± 2	57	34 ± 3
0.501	50 ± 3	0.00	5 ± 1	−3 ± 1	78	38 ± 2
T = 16.5 °C						
0.205	34 ± 1	0.32	0 ± 1	−2 ± 3	45	50 ± 3
0.327	47 ± 3	0.11	2.0 ± 1.5	−3 ± 2	37	37 ± 3
0.408	52 ± 3	0.10	6 ± 1	−4 ± 2	65	35 ± 3
0.501	50 ± 2	0.00	5 ± 1	−3.5 ± 0.5	78	37 ± 3
T = 25.0 °C						
0.205	32 ± 1	0.35	0 ± 2	−1.0 ± 1	43	54 ± 3
0.327	46 ± 2	0.11	1.8 ± 0.5	−4 ± 3	60	41 ± 3
0.408	50.6 ± 0.7	0.09	3 ± 1	−4 ± 1	60	36 ± 3
0.501	49 ± 2	0.00	5.0 ± 1.5	−3.0 ± 0.5	70	38 ± 3
T = 30.0 °C						
0.205	31 ± 1	0.32	0.5 ± 1	0.0 ± 0.5	68	59 ± 3
0.327	44 ± 1	0.13	2 ± 1	−3 ± 1	82	44 ± 3
0.408	50 ± 2	0.07	3.0 ± 1.5	−4 ± 2	95	39 ± 3
0.501	48 ± 2	0.00	4.8 ± 0.5	−4 ± 1	79	37 ± 3
T = 35.0 °C						
0.205	29 ± 2	0.41	0.1 ± 1	0 ± 1	29	55 ± 2
0.327	41 ± 2	0.16	2.0 ± 1.5	−2 ± 1	65	51 ± 3
0.408	48 ± 3	0.08	4 ± 2	−3 ± 1	70	35 ± 2
0.501	46 ± 2	0.00	5 ± 1	−4 ± 2	89	41 ± 2

Finally, for all scattering intensities of Figures 1, 2, 4−8, the coherent part of the spectrum was analyzed assuming a form factor $P(Q)$ of polydispersed spheres with a Schultz distribution of sizes (see eq 6) and the structure factor $S'(Q)$ of adhesive hard spheres, interacting via the square well Baxter's potential (see eq 3). The scattered intensity is given by eq 5.

Table 1 contains the ϕ values, the water and the surfactant volume fractions ϕ_w and ϕ_s calculated by samples compositions for each sample at 20 °C, the four fitting parameters of the AHS model, η, and the reduced χ^2 values of the fits. The Baxter model is expected to be accurate below the percolation threshold.[3] However, low χ^2 values are obtained for samples below the percolation threshold and for two samples just above the threshold. The condition $\eta > \phi_w$ is verified (see the Microemulsion Model section) when $\Delta > 0$. In Table 2, the four fitting parameters for each temperature, the η values, and the χ^2 are reported. The contrast reported in the Introduction section was maintained constant as a function of temperature in the explored thermal range.

In Tables 1 and 2, we reported also results obtained by using the Baxter model to describe the scattering intensities of samples well above the dynamic percolation threshold. This is justified by the fact that dynamic percolation describes the microemulsion system as composed by droplet clusters below and above such a threshold, being clear that the description of the dense samples is approximate. We expect that droplets in a cluster are more closely packed than those in dilute samples and stick and unstick continuously, resulting in measured diameters greater than those of the dilute region. Without being absolutely accurate, these measurements give useful information on the microstructure of dense samples.

In Figure 9, σ, Σ, Δ, and u_o are reported as a function of ϕ. σ and Δ (size and adhesivity region) increase, whereas Σ and u_o decrease (the absolute value increases) with increasing ϕ. The consequence is the increase of the surfactant packing,

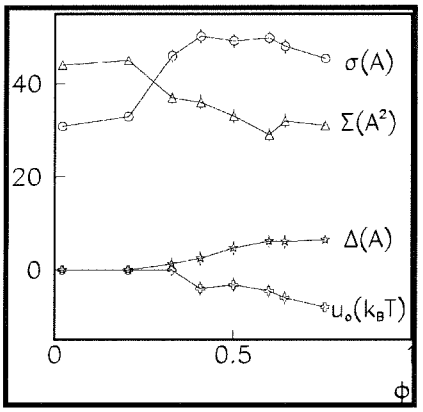

Figure 9. σ, Σ, Δ and u_o as a function of ϕ at 20 °C.

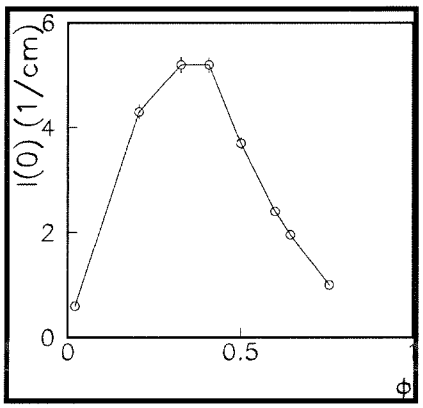

Figure 10. $I(0)$ versus ϕ.

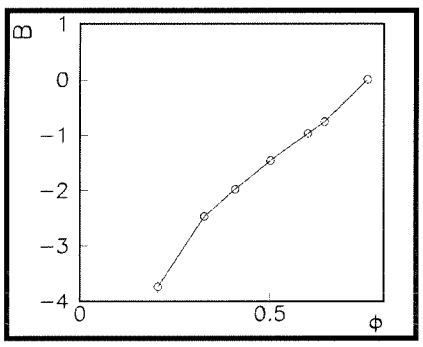

Figure 11. Second virial coefficient versus ϕ.

caused by reduction of the area per polar head at the interface, and enhancement of the adhesion between droplets.

In Figure 10, a plot of the $I(0)$ extrapolated from the fitting curves versus ϕ is reported, excluding the points at low Q due to aggregates. In the limit of $Q \rightarrow 0$, the droplet form factor is 1, and the structure factor reduces to $S(Q=0) = I(Q=0) = k_BT(\partial\phi/\partial\pi)$ at constant temperature (20 °C). In Figure 10, $I(0)$, and therefore the inverse of the osmotic compressibility $(\partial\phi/\partial\pi)$, increases for dilute samples up to the percolation threshold $\phi \approx 0.408$; thereafter, it decreases. This trend can be interpreted as a gradual transition from only steric to other interactions. From the extrapolated value of $S(Q=0)$, the virial coefficient can be evaluated by $S(0) = 1/(1 + B\phi)$, where B is the second virial coefficient.[37,38] Negative B values have been found from −3.7 to −0.76 in the ϕ range of 0.205−0.644 (see Figure 11), confirming the presence of attractive interactions between particles. In addition, the observed dependence of B on ϕ seems to indicate a dominant effect of the volume fraction compared to the limited changes in adhesion when the particles become adhesive (see Table 1 and Figure 9).

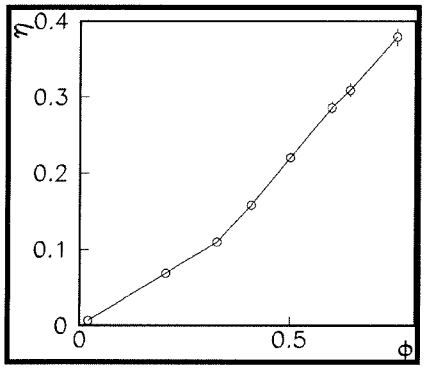

Figure 12. The η increase versus ϕ.

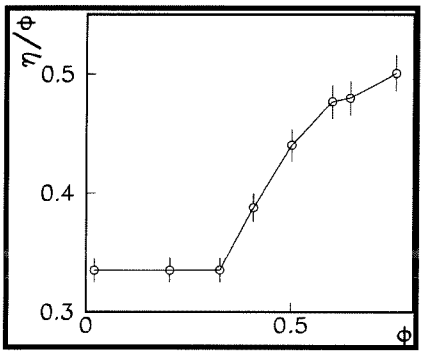

Figure 13. η/ϕ versus ϕ.

In Figure 12, η increases linearly versus ϕ, with two different slopes below and above 0.408. A discontinuity at the percolation threshold is present also for this parameter. This discontinuity is more pronounced in the plot of η/ϕ versus ϕ of Figure 13.

5. Discussion

Below $\phi = 0.408$, the microemulsion system at 20 °C is composed of droplets that interact without adhesion as Δ and u_0 are 0 within the experimental errors (two standard deviations). At 0.408, the droplets start to be adhesive as Δ and u_0 become different from 0 within the experimental errors. The σ value for dilute samples is 30 Å (polydispersity of ~30%) and increases to 46 Å close to the percolation threshold, even though the fit has a large χ^2 value. Polydispersity tends to 0 while ϕ increases from 0.408 to 0.757.

By increasing ϕ from 0.408 to 0.757, the fitted σ value increases to 45−50 Å, that is, a value larger than that for dilute samples. This value agrees well with 53 Å, that is, the distance between particles obtained for the most concentrated sample, $\phi = 0.757$, without model assumptions. For dense samples, Δ increases versus ϕ and the absolute value of u_0 as well, that is, the adhesivity increases.

It is interesting to note at this point that as soon as the particles become adhesive ($\phi \geq 0.408$), the relative range of the attractive interaction (Δ/σ) increases monotonically with increasing ϕ. The growth of such a value explains the trend of the ratio $\eta/\phi_w = (1 + \Delta/\sigma)^3$ as a function of ϕ (values of η and ϕ_w in Table 1). Since ϕ_w represents the hard-sphere volume fraction, such a ratio is equal to 1 at low ϕ, corresponding to the absence of attraction. As the droplets become increasingly adhesive, η/ϕ_w becomes quickly larger than 1 with increasing ϕ, in agreement with its cubic dependence on $1 + \Delta/\sigma$.

Droplets forming a cluster can have regions of superposition eventually caused by interdigitation of surfactant tails of neighboring droplets. These results are compatible with droplets getting more and more packed as ϕ increases, before a phase transition occurs in the system just above 0.757, as shown in the phase diagram.[5] The $\phi = 0.757$ sample is on the borderline between monophasic and the demixing region. In fact, the maximum ϕ for a face-centered cubic organization of the sample is slightly smaller than 0.750. The parameter reported in Table 1 for the 0.757 sample does not follow the trend of those at lower ϕ values above threshold. Likely, before demixing, the structural organization of the 0.757 sample changes due to the high close packing that presumably deforms the droplets.

Some known parameters can help to understand the organization of the droplets in the clusters. The surfactant polar head volume is 35. 26 Å^3;[39] thus, the diameter of the head is 4.1 Å. The polar head participates to the inner region of the droplet as the polar head scattering length density is the same as that of water, whereas the fluorinated surfactant tails are outside of the aqueous region. Furthermore, the surfactant extended tail length was found to be equal to 13 Å;[40−42] thus, for interacting droplets of the dense region, the surfactant tails interdigitate over a distance of a few Å, with 30 Å as the size of the aqueous plus polar head core and 26 Å as the length of two extended tails. Interdigitation was also found in lamellar liquid crystals formed by fluorinated surfactants of molecular weight 659 and water.[41] Instead, the 13 Å chain length mentioned above was obtained for a similar fluorinated surfactant, named *n*2 in ref 40, as the minor axis of ellipsoidal micelles, that is, without interdigitation. Thus, we can hypothesize that, during interactions of neighboring droplets, couples of droplets lead to a dimer of droplets for a certain time, with interdigitation of the surfactant molecules covering the droplets.

To further clarify the system structuring evolution, it is important to take into account the measured values of the surfactant area per polar head. In fact, the latter is 45 Å^2 at 20 °C for dilute samples ($\phi = 0.0205$ and 0.205) and decreases to 37 Å^2 at $\phi = 0.327$ and to 31 Å^2 at $\phi = 0.757$. These results show that the surfactant packing at the interface of the droplets depends on the concentration of droplets. In particular, the decrease of the area per polar head seems to imply that some interfacial surfactant molecules change their packing parameter, which is larger than 1 in the dilute microemulsion. The latter decrease can be interpreted as due to the coexistence of flat and curved interfacial regions into the samples, the flat interfaces presumably being located between two droplets that merge together and separate almost immediately (dynamic fusion) as suggested by the dynamic nature of the percolation de scribed in refs 11 and 13. The decrease of area per polar head at $\phi >$ 0.205 implies that dynamic fusion starts below the dynamic percolation threshold as also demonstrated by previous studies.[11,13]

The decrease of Σ versus ϕ, observed at 20 °C, is also found for the other temperatures (Table 2, $\phi > 0.205$). Furthermore, for dilute samples ($\phi = 0.205$ and 0.327), the temperature increase from 10 to 35 °C leads to an increase of Σ, whereas at $\phi = 0.408$ and 0.501, Σ remains constant versus temperature, in the limit of the experimental errors. Droplet fusion and an increase of surfactant packing with the formation of flat interfacial regions seem therefore to be present in the range of 10−35 °C at $\phi > 0.205$.

For the samples of Table 2, $\sigma \approx 50$ Å in the ϕ range of 0.408−0.501 at all temperatures. Below 0.408, lower σ values, ~30 Å are obtained, in agreement with measurements at 20 °C; polydispersity decreases versus ϕ for all temperatures; within two standard deviations, Δ and u_0 are close to 0 below 0.408 for $T = 10-25$ °C and different from 0 above 0.408. At 30 and 35 °C, Δ and u_0 are 0 below 0.501. We recall that, as reported

in refs 11 and 13, the threshold increases with increasing temperature, in agreement with the present SANS study.

At $\phi = 0.501$ and 0.408, Σ is independent of temperature in the limit of the experimental errors; thus, the surfactant does not change its interfacial conformation after the percolation of the droplets. On the contrary, at $\phi = 0.205$ and 0.327, Σ changes versus temperature.

6. Conclusion

The SANS analysis of the PFPE microemulsion system of this work confirms the dynamic percolation found by dielectric and conductivity studies. The size of the droplets is 30 Å below the percolation threshold and 50 Å above for the different temperatures in the range explored, 10−35 °C, suggesting that the droplets above the percolation threshold are superimposed on each other by interdigitation of the surfactant tails. We have used the wording dynamic fusion to describe a process where the droplets form dynamic dimers into droplets clusters, that is, couples of droplets stick and unstick continuously, leading to sizes of 50 Å intermediate between the single droplet size and 60 Å corresponding to two droplet sizes. The measured 50 Å intermediate size suggests that surfactant tails interdigitate between droplets. The decrease of the surface per polar head at the surface of dense microemulsion samples, with increasing concentration, obtained by measures of the Porod region of the SANS spectra, represents an independent confirmation that the surface of the system decreases as a function of concentration above the percolation threshold. This landscape is the same for all of the temperatures investigated.

Acknowledgment. Thanks are due to S.-H. Chen and F. Sciortino for helpful discussions. Criticisms and comments of A. Chittofrati, M. Monduzzi, G. Martini, and S. Ristori are also appreciated. We acknowledge Ausimont for having provided the fluorinated compounds, the EC for support via the "Human Capital and Mobility - Access to Large Scale Facilities" Program, Contract ERB CHGECT920001, and the Italian MIUR, PRIN 2005, INFM, and CSGI for financial support.

References and Notes

(1) Kahlweit M. In *Structure and Dynamics of Strongly Interacting Colloids and Supramolecular Aggregates in Solution*; Chen, S.-H., et al., Eds; NATO ASI Series C369; Kluwer Academic Publishers:The Netherlands, 1992.

(2) Kotlarchyk, M.; Chen, S.-H.; Huang, J. S.; Kim, M. W. *Phys. Rev. Lett.* **1984**, *53*, 914.

(3) Chen, S.-H.; Rouch, H.; Sciortino, F.; Tartaglia, P. *J. Phys.: Condens. Matter* **1994**, *6*, 10855.

(4) Bergenholtz, J.; Romagnoli, A. A.; Wagner, N. J. *Langmuir* **1995**, *11*, 1559.

(5) Chittofrati, A.; Lenti, D.; Sanguineti, A.; Visca, M.; Gambi, C. M. C.; Senatra, D.; Zhou, Z. *Prog. Colloid Polym. Sci.* **1989**, *79*, 218.

(6) Chittofrati, A.; Sanguineti, A.; Visca, M.; Kallay, N. *Colloids Surf.* **1992**, *63*, 219–233.

(7) Sanguineti, A.; Chittofrati, A.; Lenti, D.; Visca, M. *J. Colloid Interface Sci.* **1993**, *155*, 402.

(8) Monduzzi, M.; Chittofrati, A.; Visca, M. *Langmuir* **1992**, *8*, 1278–1284.

(9) Monduzzi, M.; Chittofrati, A.; Boselli, V. *J. Phys. Chem.* **1994**, *98*, 7591.

(10) Monduzzi, M.; Knackstedt, T.; Ninham, B. W. *J. Phys. Chem.* **1995**, *99*, 17772.

(11) Giri, M. G.; Carlà, M.; Gambi, C. M. C.; Senatra, D.; Chittofrati, A.; Sanguineti, A. *Phys. Rev. E* **1994**, *50*, 1313.

(12) Giri, M. G.; Carlà, M.; Gambi, C. M. C.; Senatra, D.; Chittofrati, A.; Sanguineti, A. *Prog. Colloid Polym. Sci.* **1996**, *100*, 182.

(13) Gambi, C. M. C.; Giri, M. G.; Carlà, M.; Senatra, D.; Chittofrati, A. *Phys. Rev. E* **1997**, *56*, 4356.

(14) Baglioni, P.; Gambi, C. M. C.; Giordano, R.; Senatra, D. *J. Mol. Struct.* **1996**, *383*, 165.

(15) Baglioni, P.; Gambi, C. M. C.; Giordano, R. *Physica B* **1997**, *234–236*, 295.

(16) Senatra, D.; Gambi, C. M. C.; Giri, M. G.; Carlà, M.; Chittofrati, A. *J. Therm. Anal. Calorim.* **1999**, *56*, 1335–1346.

(17) Carlà, M.; Gambi, C. M. C.; Giri, M. G.; Pieraccini, L.; Senatra, D.; Chittofrati, A.; Sanguineti, A. *IEEE Trans. Dielectr. Electr. Insul.* **1994**, *1*, 716.

(18) Gambi, C. M. C.; Giordano, R.; Laurati, M.; Lanzi, L.; Pini, F.; Baglioni, P. *Appl. Phys. A: Mater. Sci. Process.* **2002**, *74*, S377–S379.

(19) Eicke, H. F.; Borkovec, M.; DasGupta, D. *J. Phys. Chem.* **1989**, *93*, 314–317.

(20) Kallay, N.; Chittofrati, A. *J. Phys. Chem.* **1990**, *94*, 4755–4756.

(21) Duits, M. H. G.; May, R. P.; Vrij, A.; de Kruif, C. G. *Langmuir* **1991**, *7*, 62.

(22) Duits, M. H. G.; de Kruif, C. G.; Vrij, A. *Colloid Polym. Sci.* **1992**, *270*, 154.

(23) Robertus, C.; Philipse, W. H.; Joosten, J. G. H.; Levine, Y. K. *J. Chem. Phys.* **1989**, *90*, 4482.

(24) Huang, J. S.; Safran, S. A.; Kim, M. W.; Grest, G. S.; Kotlarchyk, M.; Quirke, N. *Phys. Rev. Lett.* **1985**, *53*, 592.

(25) Chen, S.-H.; Ku, C. Y.; Rouch, J.; Tartaglia, P.; Cametti, C.; de Samseth, J. J. *Phys. IV* **1993**, *3*, 143.

(26) Goyal, P. S.; Menon, S. V. G.; Dasannacharya, B. A.; Thiyagarajan, P. *Phys. Rev. E* **1995**, *51*, 2308.

(27) Lemaire, B.; Bothorel, P.; Roux, D. *J. Chem. Phys.* **1983**, *87*, 1023.

(28) Huang, J. S.; Safran, S. A.; Kim, M. W.; Grest, G. S.; Kotlarchyk, M.; Quirke, N. *Phys. Rev. Lett.* **1984**, *53*, 592.

(29) Baxter, R. J. *Aust. J. Phys.* **1968**, *21*, 563.

(30) Baxter, R. J. *J. Chem. Phys.* **1968**, *49*, 2770.

(31) Menon, S. V. G.; Manohar, C.; Srivasa Rao, K. *J. Chem. Phys.* **1991**, *95*, 9186.

(32) Kotlarchyk, M.; Chen, S.-H. *J. Chem. Phys.* **1983**, *79*, 2461.

(33) van Beurten, P.; Vrij, A. *J. Chem. Phys.* **1981**, *74*, 2744.

(34) Pedersen, J. S.; Posselt, D.; Mortensen, K. J. *Appl. Cryst.* **1990**, *23*, 321.

(35) Teixeira J. In *Structure and Dynamics of Strongly Interacting Colloids and Supramolecular Aggregates in Solution*; Chen, S.-H., et al., Eds.; Kluwer Academic Publishers: The Netherlands, 1992.

(36) *Small Angle X-ray Scattering*; Glatter, O., Kratky, O., Eds.; Academic Press: New York, 1982.

(37) Agterof, W. G. M.; van Zomeren, J. A. J.; Vrij, A. *Chem. Phys. Lett.* **1976**, *43*, 363.

(38) Giordano, R.; Maisano, G.; Teixeira, J. J. *Appl. Cryst.* **1990**, *30*, 761.

(39) Marcus Y. In *Ion properties*; Marcel Dekker: New York, 1997.

(40) Gambi, C. M. C.; Giordano, R.; Chittofrati, A.; Pieri, R.; Laurati, M.; Baglioni, P.; Teixeira, J. *J. Phys. Chem. B* **2007**, *111*, 1348.

(41) Gebel, G.; Ristori, S.; Loppinet, B.; Martini, G. *J. Phys. Chem.* **1993**, *97*, 8664.

(42) Mele, S.; Ninham, B. W.; Monduzzi, M. *J. Phys. Chem. B* **2004**, *108*, 17751.

JP911278J